Fluorine-vacancy defects in fluorine-implanted silicon studied by electron paramagnetic resonance

T. Umeda,[1,a)] J. Isoya,[1] T. Ohshima,[2] S. Onoda,[2] N. Morishita,[2] K. Okonogi,[3] and S. Shiratake[3]

[1]University of Tsukuba, Tsukuba 305-8573, Japan
[2]Japan Atomic Energy Agency, Takasaki 370-1292, Japan
[3]Elpida Memory, Inc., Higashihiroshima 739-0198, Japan

An electron paramagnetic resonance (EPR) study on fluorine-vacancy defects ($F_n V_m$) in fluorine-implanted silicon is demonstrated. Fluorine implantation is an important technology for Si microdevices and EPR measurements showed that this process created a variety of $F_n V_m$ defects of different sizes (V_2, V_4, and V_5). In $F_n V_m$, a Si–F bond exhibited a different chemical nature compared to a Si–H bond in hydrogen-vacancy complexes. The most primitive defect was $F V_2$ (F0 center) and the final types were $F_n V_5$ (F1 center) and $F_n V_2$ (F2 center) which increased in annealing processes as low temperature as 200 °C. © 2010 American Institute of Physics. [doi:10.1063/1.3473763]

Fluorine forms a strong bond with silicon,[1] similar to hydrogen (Si–H), which is useful for Si technologies.[2] Fluorine also has great benefits for suppressing transient enhanced diffusion of boron atoms.[1,3–6] This property is believed to be due to the formation of fluorine-vacancy defects ($F_n V_m$), which suppress the activity of interstitial (I)-type defects interacting with boron atoms.[1,3,4] First-principles calculations predicted that the most stable $F_n V_m$ defects are $F_4 V$ or $F_6 V_2$ which are fully passivated by F atoms.[1,3,4] On the other hand, positron annihilation spectroscopy (PAS) revealed two preferential sizes of vacancies (approximately V_2 or V_4).[5,6] Secondary ion mass spectroscopy showed a high threshold temperature ($\sim$550 °C) for fluorine diffusion,[5] suggesting that F atoms become immobile due to strong Si–F bonds in $F_n V_m$.[1]

In this Letter, we present a different approach to investigate fluorine and $F_n V_m$ defects using electron paramagnetic resonance (EPR), which provides a more concrete view of fluorine behaviors in Si. We found at least four types of paramagnetic $F_n V_m$ defects of different sizes (V_2, V_4, and V_5) in as-implanted and in subsequently annealed Si. Using EPR, their behavior could be studied individually as follows: (1) two distinct types (V_2 and V_5) were stable, providing microscopic models for the previous PAS data, (2) a different nature of the Si–F bond was found in comparison with the Si–H bond, and (3) low-temperature motion ($<$20 °C) and diffusion ($\sim$200 °C) of $F_n V_m$ were revealed.

The starting substrates ($0.3 \times 0.8 \times 0.01$ cm^3) were phosphorus-doped float zone Si(100) with a high resistivity ($>$1000 Ω cm) and integrated-circuits-grade 30-cm-diameter Czochralski-Si(100) with an epitaxial layer and phosphorus or boron doping (5–15 Ω cm). For the former wafers, multiple F implantation was performed on both of their wide faces by 5×10^{11} to 5×10^{14} F/cm^2 with 7.5 to 15 MeV, which was designed for high-sensitive EPR measurements. A more realistic (shallow and single) F implantation[2,3,6] was examined on the latter wafers by 1×10^{12} to 1×10^{14} F/cm^2 with 20 keV. These two processes created F profiles as shown in the inset of Fig. 1. After di-

luted hydrogen fluoride treatments on the sample surfaces, EPR spectra were measured using a Bruker Bio-Spin E500 X-band spectrometer with 100 kHz magnetic-field modulation of 0.05 to 0.1 mT width.

EPR spectra of six samples are shown in Figs. 1(a)–1(e). In the lowest-dose sample (a), no significant effects of F were detected. The spectrum is dominated by the well-
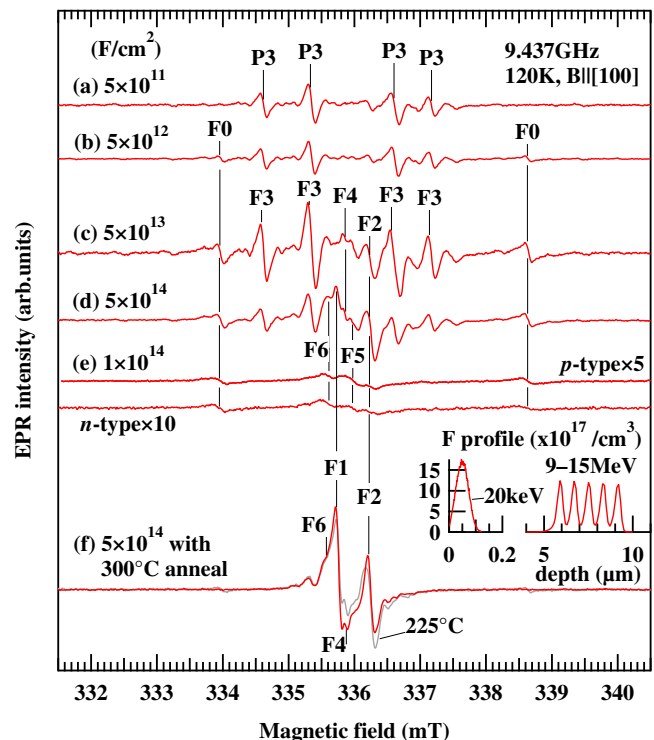

FIG. 1. (Color online) EPR spectra of F-implanted Si. F doses are (a) 5×10^{11} F/cm^2 at 6 energies, (b) 5×10^{12} F/cm^2 at 5 energies, (c) 5×10^{13} F/cm^2 at 5 energies, (d) 5×10^{14} F/cm^2 at 3 energies, (e) 1×10^{14} F/cm^2 at 20 keV (for p- and n-type wafers), and (f) with isochronal annealing (225 and 300 °C). The inset shows F profiles for the 20 keV (1×10^{13} F/cm^2) and high-energies (5×10^{13} F/cm^2) implantations simulated by the SRIM code. Peak F densities are (a) 1.2×10^{16}, (b) 1.2×10^{17}, (c) 1.2×10^{18}, (d) 1.2×10^{19}, and (e) 1.7×10^{19} F/cm^3. Labels of F0 to F6 indicate a series of new EPR centers originating from $F_n V_m$ defects. In (a) and (b), a weak signal at 336.2 mT was different from F2, judging from its isotropic angular dependence. It is probably due to a surface-damage center.
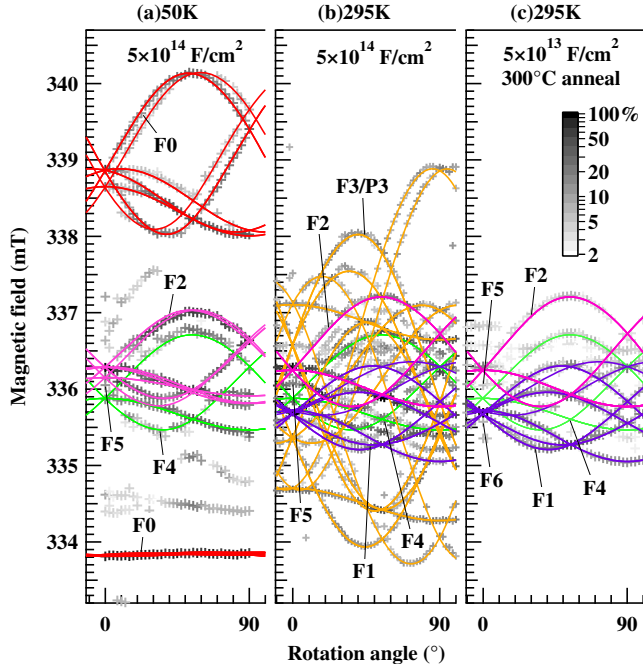
a)Electronic mail: umeda@bk.tsukuba.ac.jp.

FIG. 2. (Color online) Angular maps of F0–F4 centers (F_nV_m defects) at 9.437 GHz. Magnetic field was rotated from [100] (0°) to [011] (90°). Gray symbols indicate experimental peak positions and their normalized intensities (the largest peak=100%) are expressed by a gray scale shown in inset. Solid lines are simulated by SH parameters in Table I. There are still untraced angular maps (e.g., F5 and F6), suggesting more variety of minor F_nV_m defects.

known P3 center (neutral {110}-planar V_4 chain, an electron spin $S=1$).[7–9] I-type defects such as P6 (I_2), H8 (I-related), and B3/4/5 (I_{3-4}) (Refs. [7–9]) were not detected in our as-implanted samples or in the annealing study. In the next sample (b), a doublet signal with $S=1/2$ was observed. This doublet is ascribed as a hyperfine splitting (hfs) of ^{19}F (nuclear spin $I=1/2$, natural abundance=100%). We named this "F0." Following to F0, other signals labeled "F1" to "F6" were observed in (c)–(e). These signals are most probably due to subsequent defects of F0 that are associated with more vacancies and/or F atoms. Basically, such a formation behavior was common to the deep implantations (b)−(d) and shallow implantations (e), except the absence of the F3 sig-

nal in (e). A reason for this absence will be presented later.

The F0 spectrum was not detectable above 200 K, and it exhibited a thermally activated reorientation behavior above 60 K. Thus, in Fig. 2(a), the angular map of F0 is examined at 50 K. The F0 center shows two separated patterns due to a ^{19}F hfs with monoclinic-I symmetry close to trigonal one. Just in the middle of the F0's patterns, a F2 pattern with the same symmetry was observed. Table I shows the determined spin-Hamiltonian (SH) parameters of F0 and F2. Both centers have similar g tensors of P_b-center-like ($g_X \approx g_Y \equiv g_\perp \approx 2.007$, $g_Z \equiv g_\parallel \approx 2.001$, the $g_\parallel$ axis is nearly parallel to $\langle 111 \rangle$), indicating neutral Si dangling-bond (DB) nature for both origins. The F2 spectrum became larger with higher F doses [Fig. 1(d)] and still larger after annealing such that F0 decreased or vanished [Fig. 1(f)]. This suggests that F2 is a subsequent defect of F0 with more accumulation of F atoms. The major difference between F0 and F2 is ^{19}F hfs. The ^{19}F hyperfine tensor (**A**) of F0 shows an axial symmetry due to an F $2p$ orbital that is parallel to the $g_\parallel$ axis (i.e., the DB orbital). We constructed neutral F_nV_2 models, based on all the data, for the origins of F0 ($n=1$) and F2 ($n=2-5$). The respective models are shown in Figs. 3(a) and 3(b). They can reasonably account for all the facts as follows. (1) FV_2 [Fig. 3(a)] contains a single neutral DB ($S=1/2$) as well as (2) a single Si–F bond parallel to the DB orbital. (3) The V_2 distance (0.59 nm) allows a weak bond to form between the DB and F atom [Fig. 3(a)], extending the spin density over the ^{19}F atom. (4) However, this weak bond will be broken if F atoms are then added into the vacancy [Fig. 3(b)]. (5) This mechanism controls the appearance of ^{19}F hfs, resulting in the two distinguishable F_nV_2 centers. (6) As similarly to V_2 (the G6 center) at 40–110 K,[10] a thermally activated rearrangement can be expected for F0 among three equivalent DB-F pairs (Si_1-F-Si_4, Si_2-F-Si_5, and Si_3-F-Si_6),[11] causing the characteristic temperature dependence at 60–150 K. At higher temperatures (>200 K), F atoms seemed to move inside the vacancy, resulting in the broadening and disappearance of F0 as well as a trigonal average of F2 [see Figs. 2(b) and 2(c), Table I]. Such a motion was also observed for hydrogen in a vacancy (>200 K).[12]

It is quite interesting to compare the F0/F2 centers (neutral F_nV_2) with neutral hydrogen-vacancy defects[12] such as

TABLE I. SH parameters of F_nV_m defects and related V-type defects. Total SH is given by $H = \mu_B \mathbf{S} \cdot \mathbf{g} \cdot \mathbf{B} + \mathbf{S} \cdot \mathbf{D} \cdot \mathbf{S} + \mathbf{S} \cdot \mathbf{A} \cdot \mathbf{I} - g_n \beta_n \mathbf{I} \cdot \mathbf{B}$, where **g** is a g tensor, **D** is a fine interaction tensor (excluded for spin-1/2 centers), and **A** is a hyperfine tensor (included only for F0 and S1a) (Refs. [7–9] and [12]). Principal values of **A** and **D** are expressed in mT. **D** and **g** tensors of F3 and P3 are identical. (m) and (t) denotes monoclinic-I and trigonal symmetries. Measured temperatures are specified only for temperature-dependent spectra. Anneal and growth temperatures (signal was reduced or increased in these ranges, respectively), are also summarized.

Center	S	Tensor	X	Y	$Z(\parallel)$	θ	Anneal/growth temperature
F0 (FV_2^0)	1/2 (m)	**g**(50 K)	2.0070	2.0067	2.0006	30.2°	220–280 °C/none
		A(^{19}F) [a]	4.23	4.15	6.27	210.4°	
F2 ($F_nV_2^0$)	1/2 (m)	**g**(50 K)	2.0080	2.0072	2.0005	32.9°	300–over 410 °C/200–300 °C
	1/2 (t)	**g**(295 K)	2.0081	2.0081	1.9995	35.26°	
S1a (HV_2^0)	1/2 (m)	**g**(200 K)	2.0110	2.0100	2.0008	31.0°	180–280 °C/none [b]
		A(^1H) [a]	0.050	0.057	0.13	4.5°	
F3 ($F_nV_4^0$)	1 (m)	**g**	2.0102	2.0099	2.0010	34.4°	F3: 200–230 °C/none
P3 (V_4^0)	1 (m)	**D**	−8.34	−7.92	16.26	−6.3°	P3: 120–170 °C/none [c]
F1 (F_nV_5)	1/2 (m)	**g**(295 K)	2.0088	2.0124	2.0046	17.5°	300–over 410 °C/200–300 °C
P1 (V_5)	1/2 (m)	**g**(320 K)	2.0091	2.0127	2.0050	15.0°	300–460 °C/120–250 °C [d]
F4	1/2 (t)	**g**	2.0112	2.0112	2.0019	35.26°	250–over 410 °C/200–250 °C

[a]Absolute values.
[b]Reference 12.
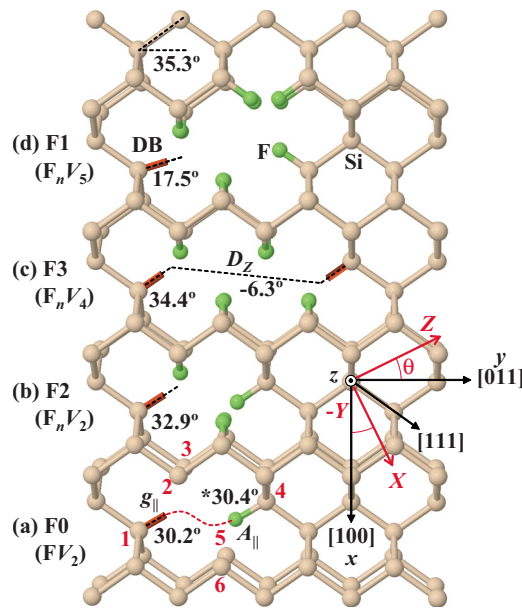[c]References 7 and 9.
[d]Reference 8.

FIG. 3. (Color online) Atomic models for F0–F3 centers drawn in the Si($0\bar{1}1$) plane. Cartesian coordinates (xyz) and principal coordinates of SH tensors (XYZ) are also defined. Angles θ are shown for main principal directions (Z or $\parallel$) of **g**, **A**, and **D** tensors. F0, F1, and F2 have a single DB ($S=1/2$), while F3 contains two DBs ($S=1$). In (a), a weak bond between DB and F atom is drawn by a dashed line, which generates ^{19}F hfs. $^*\theta$ angle from the -*y* axis.

HV_2 (the S1a center). Table I shows that their g tensors belong to the same class. However, interestingly, there is a big difference between H and F. Hydrogen and DB does not form a weak bond even in a monovacancy (HV). Therefore, both the HV and HV_2 spectra revealed only very weak point-dipole interaction of ^{1}H nuclear spin ($I=1/2$, natural abundance=99.9%),[12] which is one or two orders of magnitude weaker than the ^{19}F hyperfine interaction of FV_2 [**A**(^{1}H) values are 0.1–0.3 mT for HV (Ref. 12), and also see Table I for HV_2 and FV_2]. The observed ^{19}F hfs can be explained by the direct distribution of the spin density on ^{19}F. The formation of a weak bond between the DB and F atom enables this. Based on the standard linear combination of atomic orbitals analysis,[13] 1.4% of the spin density (F $2s$ =0.25% and F $2p=1.1\%$) is estimated on the F atom for F0.

Note that the F0 center is one of the most primitive defects due to F implantation. In the 5×10^{12} F/cm^2 sample [Fig. 1(b)], 48% of F atoms ($48\%\times5\times10^{12}\times10$ F/cm^2) were consumed by F0 (FV_2). Previous PAS studies also revealed V_2-type defects (S-parameter=1.04) in their as-implanted samples.[5,6]

With an increased F dose, we could clearly detect the F1 and F3 spectra. A typical F3 spectrum was observed in the 5×10^{13} F/cm^2 sample [Fig. 1(c)]. Its angular pattern [Fig. 2(b)] and SH parameters are indistinguishable from those of the P3 center (V_4^0). However, in the isochronal anneal study (30 min at 25 °C step), we found a higher thermal stability for F3 (annealed at 200–230 °C) compared to P3 (120–170 °C.[7,9]) Therefore, we suggest that the F3 center accumulates F atoms into V_4. Our proposed model for F3 is shown in Fig. 3(c). Since $S=1$ for F3, there should be two neutral Si DBs separated by the V_4 distance (0.97 nm). Since these DBs could be easily charged with doping for the case

of P3,[7] the F3 spectrum could disappear in the n- and p-type samples [Fig. 1(e)]. It is notable that F_nV_4 (F3) was less stable than F_nV_2 (F2), because the F2 spectrum remained after F3 completely vanished [at 225 and 300 °C, Fig. 1(f)]. F_nV_4 seems to be decomposed into F_nV_2.

In the isochronal annealing study, the most stable center was "F1." A typical spectrum for it appears in Fig. 1(f). The angular map of F1 is clearly traced in Fig. 2(c). The determined g tensor of F1 was close to that of the P1 center.[7,8] The P1 center has a single neutral DB ($S=1/2$) and has been identified as a negative nonplanar V_5 cluster.[8] Based on the P1 model, we assign the F_nV_5 model to the origin of F1, as shown in Fig. 3(d). In the 5×10^{14}-F/cm^2 sample, the density of F1 was maximized to 1.3×10^{14}/cm^2 after 300 °C anneal. In this situation, if one assumes 50% decoration of F atoms for F1 (six F atoms/V_5), 52% of implanted F atoms (52% $\times5\times10^{14}\times6$ F/cm^2) would accumulate into F1. Further annealing decreased the F1 centers, however, they were stable and remained by 8×10^{14}/cm^2 at 410 °C. In previous PAS studies, the maximum vacancy size was found to be about V_4 (S-parameter=1.05) after 700 °C annealing.[5] The F1 center is the most probable candidate for such large, stable defects.

In summary, using EPR, we found a variety of F_nV_m defects (F0–F6) in F-implanted Si and in the subsequent annealing study. The most primitive center was FV_2 (the F0 center) observed in the initial stage of F implantation and this center revealed a characteristic ^{19}F hfs. With increasing the F dose or annealing the sample, other F_nV_m defects with more accumulation of F atoms were observed. The most stable center was the F1 center (F_nV_5), and the next one was the F2 center (F_nV_2). F_nV_3 defects were not found. F_nV_4 defects were probably detected as the F3 center.

[1]M. Diebel and S. T. Dunham, Phys. Rev. Lett. **93**, 245901 (2004).

[2]Y. I. Kim, K. H. Yang, and W. S. Lee, IEEE Int. Reliab. Phys. Symp. Proc. **2004**, 667; K. Ohyu, T. Umeda, K. Okonogi, S. Tsukada, M. Hidaka, S. Fujieda, and Y. Mochizuki, Tech. Dig. - Int. Electron Devices Meet. **2006**, 389.

[3]G. M. Lopez, V. Fiorentini, G. Impellizzeri, S. Mirabella, and E. Napolitani, Phys. Rev. B **72**, 045219 (2005).

[4]G. M. Lopez and V. Fiorentini, Appl. Phys. Lett. **89**, 092113 (2006).

[5]X. D. Pi, V. P. Burrows, and P. G. Coleman, Phys. Rev. Lett. **90**, 155901 (2003).

[6]P. J. Simpson, Z. Jenei, P. Asoka-Kumar, R. R. Robison, and M. E. Law, Appl. Phys. Lett. **85**, 1538 (2004).

[7]Y. H. Lee, Y. M. Kim, and J. W. Corbett, Radiat. Eff. **15**, 77 (1972).

[8]Y. H. Lee and J. W. Corbett, Phys. Rev. B **9**, 4351 (1974).

[9]D. Pierreux and A. Stesmans, Phys. Rev. B **71**, 115204 (2005).

[10]G. D. Watkins and J. W. Corbett, Phys. Rev. **138**, A543 (1965).

[11]In this model, we predict a "cooperative" jump of a DB and a F atom. This feature will be also as a consequence of the weak-bond formation in FV_2. In fact, the HV_2 center, which has an atomic structure just analogue to FV_2, did not show such a motional effect (Ref. 12), most probably because there was no weak bond between a DB and a H atom.

[12]B. Bech Nielsen, P. Johannesen, P. Stallinga, and K. Bonde Nielsen, Phys. Rev. Lett. **79**, 1507 (1997); P. Stallinga, P. Johannesen, S. Herstrøm, K. B. Nielsen, B. Bech Nielsen, and J. R. Byberg, Phys. Rev. B **58**, 3842 (1998).

[13]J. A. Weil, J. R. Bolton, and J. E. Wertz, *Electron Paramagnetic Resonance* (Wiley, New York, 1994).